

Table 7-1. Mineral classes

| Class | Chemical characteristics | Examples |
|--|--|---|
| Borates | Various elements in combination with boron | Borax [$\text{Na}_2\text{B}_4\text{O}_7 \cdot 10\text{H}_2\text{O}$] |
| Carbonates | Metals in combination with carbonate (CO_3^{2-}) | Calcite [CaCO_3] Cerrusite [PbCO_3] |
| Halides | Alkali metals or alkaline earths in combination with halogens (F, Cl, Br, I) | Halite [NaCl] Fluorite [CaF_2] |
| Hydroxides | Metals in combination with hydroxyls (OH^-) | Brucite [$\text{Mg}(\text{OH})_2$] |
| Native elements | Pure compound of a metallic or nonmetallic element | Gold [Au] Graphite [C] |
| Oxides | Metals in combination with oxygen | Hematite [Fe_3O_4] |
| Phosphates, arsenates, vanadates, chromates, tungstates & molybdates | Various elements in combination with the ZO_4 radical where Z = P, As, V, Cr, W, Mo | Apatite [$\text{Ca}_5(\text{PO}_4)_3(\text{F}, \text{Cl}, \text{OH})$] Carnotite [$\text{K}_2(\text{UO}_2(\text{VO}_4)_2 \cdot 3\text{H}_2\text{O})$] Scheelite [CaWO_4] |
| Silicates | Metals in combination with silica tetrahedra (SiO_4^{4-}) for ming three dimensional networks, sheets, chains and isolated tetrahedra | Quartz [SiO_2] Forsterite [MgSiO_4] Orthoclase [KAlSi_3O_8] |
| Sulfates | Alkaline earths or metals in combination with sulfate (SO_4^{2-}) | Barite [BaSO_4] Epsomite [$\text{MgSO}_4 \cdot 7\text{H}_2\text{O}$] |
| Sulfides | One or more metals in combination with reduced sulfur or chemically similar elements (As, Se, Te) | Pyrite [FeS_2] Galena [PbS] Skutterudite [CoAs_3] |

Table 7-2. Electronegativities

| Z | Ion | Electro- negativity | Z | Ion | Electro- negativity | Z | Ion | Electro- negativity |
|----|------------------|------------------------|----|------------------|------------------------|----|------------------|------------------------|
| 1 | H ⁺ | 2.20 | 33 | As ⁵⁺ | 2.18 | 65 | Dy ³⁺ | 1.22 |
| 3 | Li ⁺ | 0.98 | 34 | Se ²⁻ | 2.55 | 67 | Ho ³⁺ | 1.23 |
| 4 | Be ²⁺ | 1.57 | 35 | Br ⁻ | 2.96 | 68 | Er ³⁺ | 1.24 |
| 5 | B ³⁺ | 2.04 | 37 | Rb ⁺ | 0.82 | 69 | Tm ³⁺ | 1.25 |
| 6 | C ⁴⁺ | 2.55 | 38 | Sr ²⁺ | 0.95 | 70 | Yb ³⁺ | --- |
| 7 | N ⁵⁺ | 3.04 | 39 | Y ³⁺ | 1.22 | 71 | Lu ³⁺ | 1.0 |
| 8 | O ²⁻ | 3.44 | 40 | Zr ⁴⁺ | 1.33 | 72 | Hf ⁴⁺ | 1.3 |
| 9 | F ⁻ | 3.98 | 41 | Nb ⁵⁺ | 1.6 | 73 | Ta ⁵⁺ | 1.5 |
| 11 | Na ⁺ | 0.93 | 42 | Mo ⁶⁺ | 2.16 | 74 | W ⁶⁺ | 1.7 |
| 12 | Mg ²⁺ | 1.31 | 43 | Tc ²⁺ | 2.10 | 75 | Re ⁷⁺ | 1.9 |
| 13 | Al ³⁺ | 1.61 | 44 | Ru ²⁺ | 2.2 | 76 | Os ⁶⁺ | 2.2 |
| 14 | Si ⁴⁺ | 1.90 | 45 | Rh ²⁺ | 2.28 | 77 | Ir ⁶⁺ | 2.2 |
| 15 | P ⁵⁺ | 2.19 | 46 | Pd ²⁺ | 2.20 | 78 | Pt ⁴⁺ | 2.2 |
| 16 | S ²⁻ | 2.58 | 47 | Ag ⁺ | 1.93 | 79 | Au ⁺ | 2.4 |
| 17 | Cl ⁻ | 3.16 | 48 | Cd ²⁺ | 1.69 | 80 | Hg ²⁺ | 1.9 |
| 19 | K ⁺ | 0.82 | 49 | In ³⁺ | 1.78 | 81 | Tl ³⁺ | 1.8 |
| 20 | Ca ²⁺ | 1.00 | 50 | Sn ²⁺ | 1.96 | 82 | Pb ²⁺ | 1.8 |
| 21 | Sc ³⁺ | 1.36 | 51 | Sb ⁵⁺ | 2.05 | 83 | Bi ³⁺ | 1.9 |
| 22 | Ti ⁴⁺ | 1.54 | 52 | Te ²⁻ | 2.1 | 84 | Po ⁴⁺ | 2.0 |
| 23 | V ³⁺ | 1.63 | 53 | I ⁻ | 2.66 | 85 | At ⁵⁺ | 2.2 |
| 24 | Cr ³⁺ | 1.66 | 55 | Cs ⁺ | 0.79 | 87 | Fr ⁺ | 0.7 |
| 25 | Mn ²⁺ | 1.55 | 56 | Ba ²⁺ | 0.89 | 88 | Ra ²⁺ | 0.9 |
| 26 | Fe ²⁺ | 1.83 | 57 | La ³⁺ | 1.10 | 89 | Ac ³⁺ | 1.1 |
| 27 | Co ²⁺ | 1.88 | 58 | Ce ³⁺ | 1.12 | 90 | Th ⁴⁺ | 1.3 |
| 28 | Ni ²⁺ | 1.91 | 59 | Pr ³⁺ | 1.13 | 91 | Pa ⁴⁺ | 1.5 |
| 29 | Cu ⁺ | 1.90 | 60 | Nd ³⁺ | 1.14 | 92 | U ⁶⁺ | 1.7 |
| 30 | Zn ²⁺ | 1.65 | 62 | Sm ³⁺ | 1.17 | 93 | Np ³⁺ | 1.3 |
| 31 | Ga ³⁺ | 1.81 | 64 | Gd ³⁺ | 1.20 | 94 | Pu ⁴⁺ | 1.3 |
| 32 | Ge ⁴⁺ | 2.01 | | | | | | |

Table 7-3. Percent ionic character of a single chemical bond

| Difference in electronegativity | Ionic character, % | Difference in electronegativity | Ionic character, % |
|---------------------------------|--------------------|---------------------------------|--------------------|
| 0.1 | 0.5 | 1.7 | 51 |
| 0.2 | 1 | 1.8 | 55 |
| 0.3 | 2 | 1.9 | 59 |
| 0.4 | 4 | 2.0 | 63 |
| 0.5 | 6 | 2.1 | 67 |
| 0.6 | 9 | 2.2 | 70 |
| 0.7 | 12 | 2.3 | 74 |
| 0.8 | 15 | 2.4 | 76 |
| 0.9 | 19 | 2.5 | 79 |
| 1.0 | 22 | 2.6 | 82 |
| 1.1 | 26 | 2.7 | 84 |
| 1.2 | 30 | 2.8 | 86 |
| 1.3 | 34 | 2.9 | 88 |
| 1.4 | 39 | 3.0 | 89 |
| 1.5 | 43 | 3.1 | 91 |
| 1.6 | 47 | 3.2 | 92 |

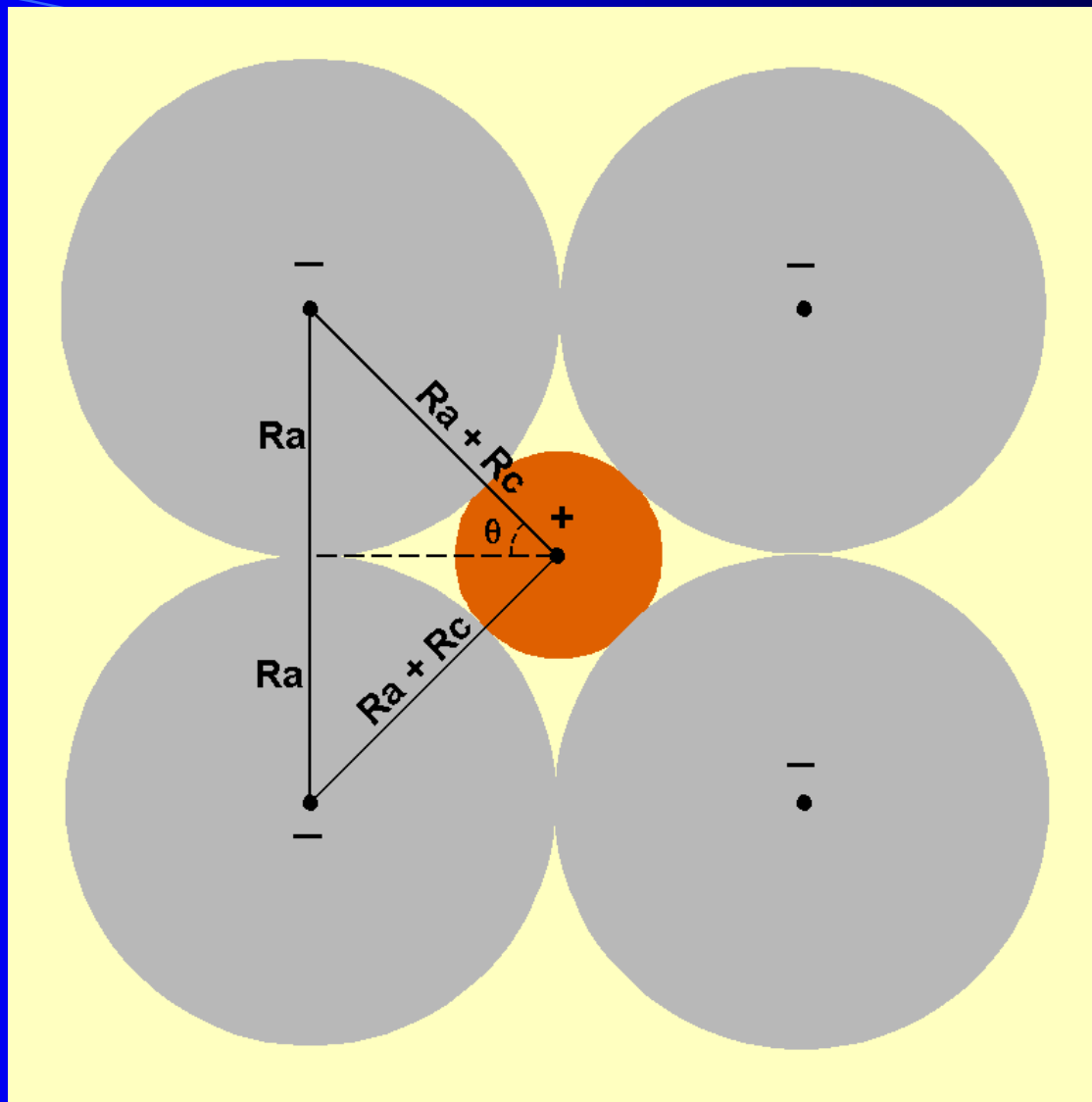
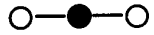
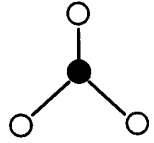
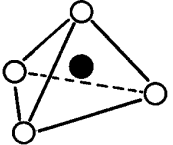
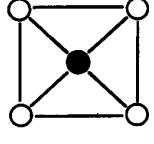
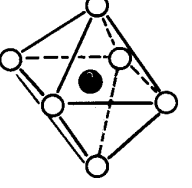
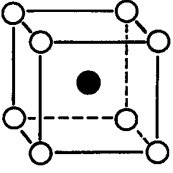
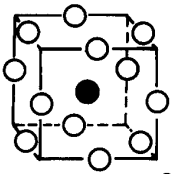


Figure 7-1. Packing of anions around a cation for a coordination number of 4. The minimum radius ratio can be calculated from the geometry of the packing. R_a and R_c are the radii of the anion and cation, respectively. In this case, $\theta = 45^\circ$. See text for calculation.

Figure 7-2. Possible arrangement of ions in crystals for particular coordination numbers (CN). Radius ratio range is listed for each CN. From Faure (1998).

| Radius ratio | Coordination | Arrangement of ions | |
|--------------|--------------|---|---------------------|
| <0.155 | 2 |  | Linear |
| 0.155–0.225 | 3 |  | Trigonal planar |
| 0.225–0.414 | 4 |  | Tetrahedral |
| 0.414–0.732 | 4 |  | Square planar |
| 0.414–0.732 | 6 |  | Octahedral |
| 0.732–1.00 | 8 |  | Body-centered cubic |
| >1.00 | 12 |  | Edge-centered cubic |

● Cation, ○ Anion

Incident x-rays

Diffracted x-rays

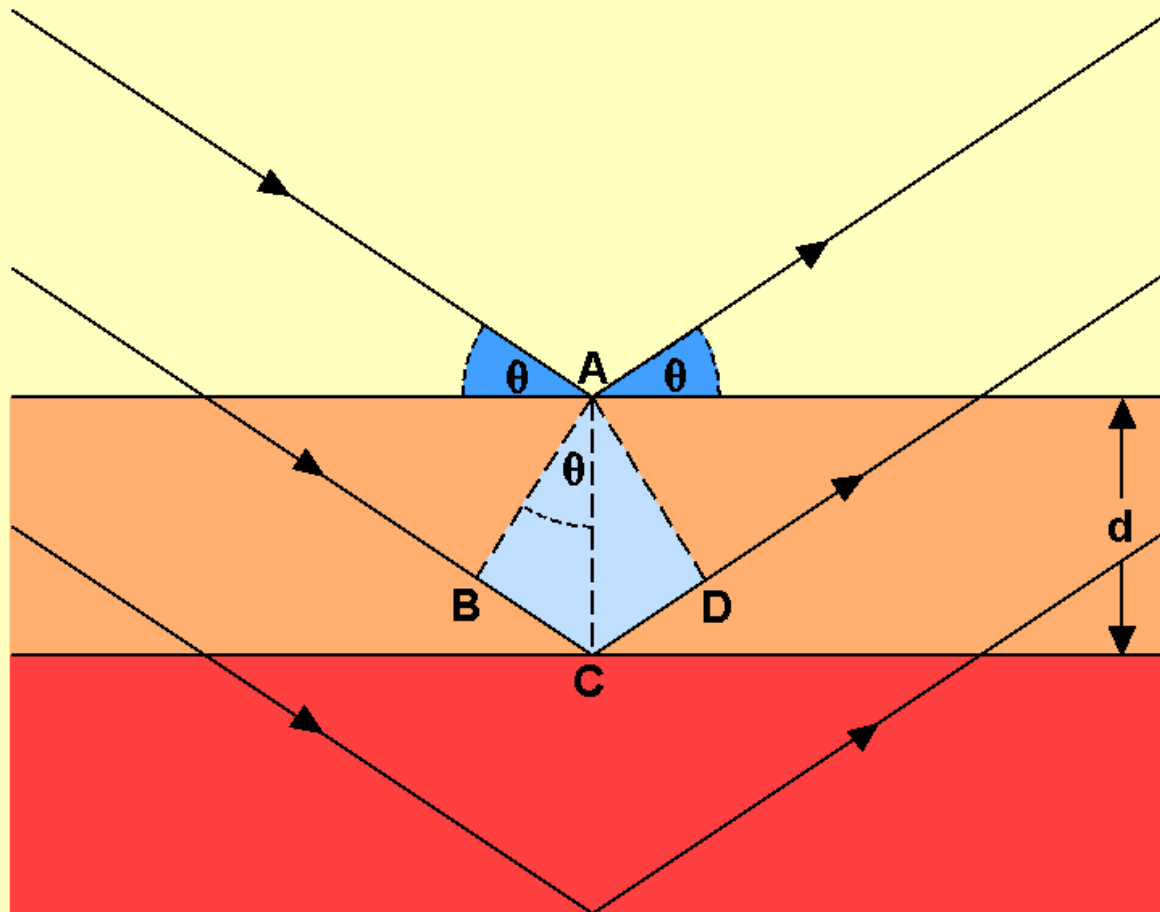


Figure 7-3. Diagram illustrating Bragg's law. θ = angle of incidence and diffraction when Bragg's law conditions are met. d = interplanar spacing.

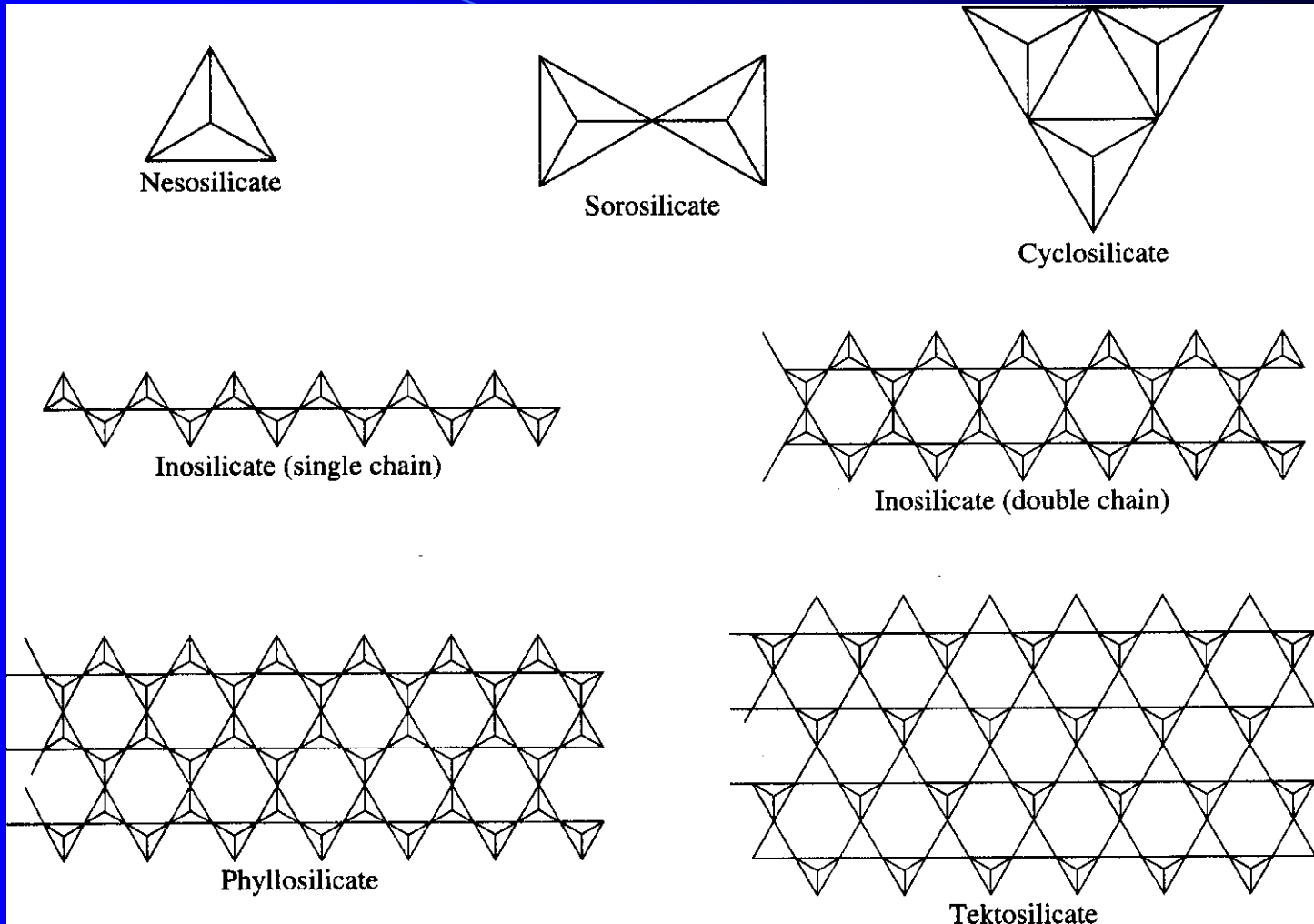
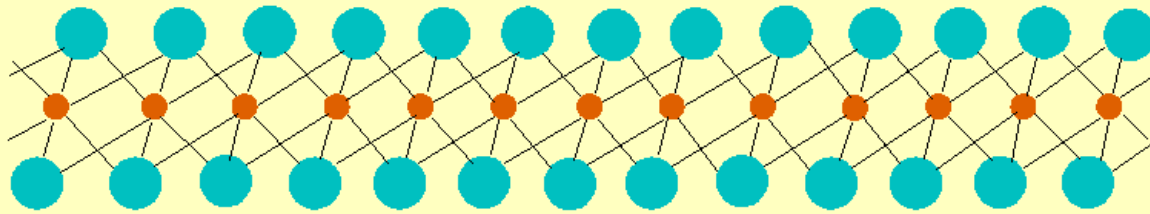


Figure 7-4. Arrangement of silica tetrahedra in the various classes of silicate minerals. See text for further discussion. From Brownlow (1996).

Table 7-4. Properties of the silicate crystal classes

| Class | Tetrahedral arrangement | # shared corners | Chemical unit | Si:O | Example |
|----------------|---|------------------|---------------------------------|--------|------------|
| Nesosilicate | Independent tetrahedra | 0 | SiO_4^{4-} | 1:4 | Olivine |
| Sorosilicate | Two tetrahedra sharing a corner | 1 | $\text{Si}_2\text{O}_7^{6-}$ | 1:3.5 | Melilite |
| Cyclosilicate | Three or more tetrahedra sharing two corners, forming a ring | 2 | SiO_3^{3-} | 1:3 | Beryl |
| Inosilicate | Single chain of tetrahedra sharing two corners | 2 | SiO_3^{3-} | 1:3 | Augite |
| | Double chain of tetrahedra alternately sharing two or three corners | 2.5 | $\text{Si}_4\text{O}_{11}^{6-}$ | 1:2.75 | Hornblende |
| Phyllosilicate | Sheet of tetrahedra sharing three corners | 3 | $\text{Si}_2\text{O}_5^{2-}$ | 1:2.5 | Kaolinite |
| Tektosilicate | Framework of tetrahedra sharing all four corners | 4 | SiO_2 | 1:2 | K-feldspar |

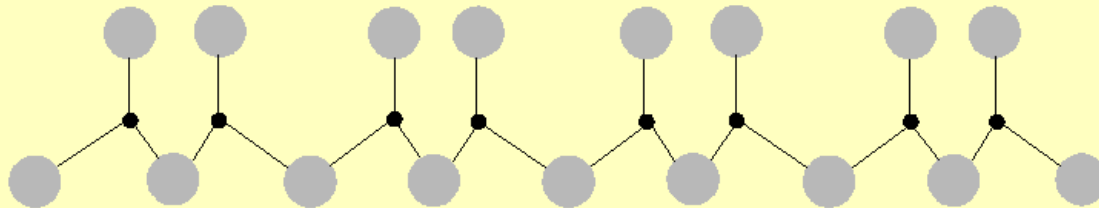
Octahedral layer



● Hydroxyl

● Mg²⁺ or Al³⁺

Tetrahedral layer



● Oxygen

● Silicon

Figure 7-5. Structure of the octahedral and tetrahedral layer. Mg²⁺ in the octahedral layer = brucite. Al³⁺ in the octahedral layer = gibbsite. Al³⁺ can substitute for Si⁴⁺ in the tetrahedral layer.

Table 7-5. Summary of the principal characteristics of the layered clay mineral groups

| | Kaolinites | Illites | Smectites | Vermiculites |
|--|---|---|--|--|
| Structure Tetrahedral: Octahedral | 1:1 | 2:1 | 2:1 | 2:1 |
| Octahedral layer | Di-octahedral | Mostly di-octahedral | Di- or tri-octahedral | Mostly tri-octahedral |
| Interlayer cations | Nil | K | Ca, Na | Mg |
| Interlayer water | Only in halloysite | Some in hydromuscovite | Ca, two layers Na, one to many layers | Ca, two layers K, one layer to nil |
| Basal spacing | 7.1 Å | 10 Å | Variable most ~15 Å | Variable 14.4 Å when fully hydrated |
| Ethylene glycol | Only taken up by halloysite | No effect | Two glycol layers, 17 Å | One glycol layer, 14 Å |
| Cation exchange capacity (CEC) in meq/100 g clay | Nil 3 - 15 | Low 10 - 40 | High 80 - 150 | High 100 - 150 |
| Formula | $\text{Al}_2\text{Si}_2\text{O}_5(\text{OH})_2$, little variation | $\text{K}_{0.5-0.75}\text{Al}_2(\text{Si},\text{Al})_2\text{O}_{10}(\text{OH})_2$ | $\text{M}^{+}_{0.7}(\text{Y}^{3+}, \text{Y}^{2+})_{4-6}(\text{Si}, \text{Al})_8\text{O}_{20}(\text{OH})_4 \cdot n\text{H}_2\text{O}$ | $\text{M}^{2+}_{0.66}(\text{Y}^{2+}, \text{Y}^{3+})_6(\text{Si}, \text{Al})_8\text{O}_{20}(\text{OH})_4 \cdot 8\text{H}_2\text{O}$ |
| Dilute acids | Scarcely soluble | Readily attacked | Attacked | Readily attacked |
| Heating 200 °C | Except halloysite, unchanged | No marked change | Collapse to approximately 10 Å | Exfoliation, shrinkage of layer spacing |
| Examples | Kaolinite, dickite, nacrite, halloysite | Illite, hydrous micas, phengite, brammallite, glauconite, celadonite | Montmorillonite, beidellite, nontronite, hectorite, saponite, saucanite | Vermiculite |

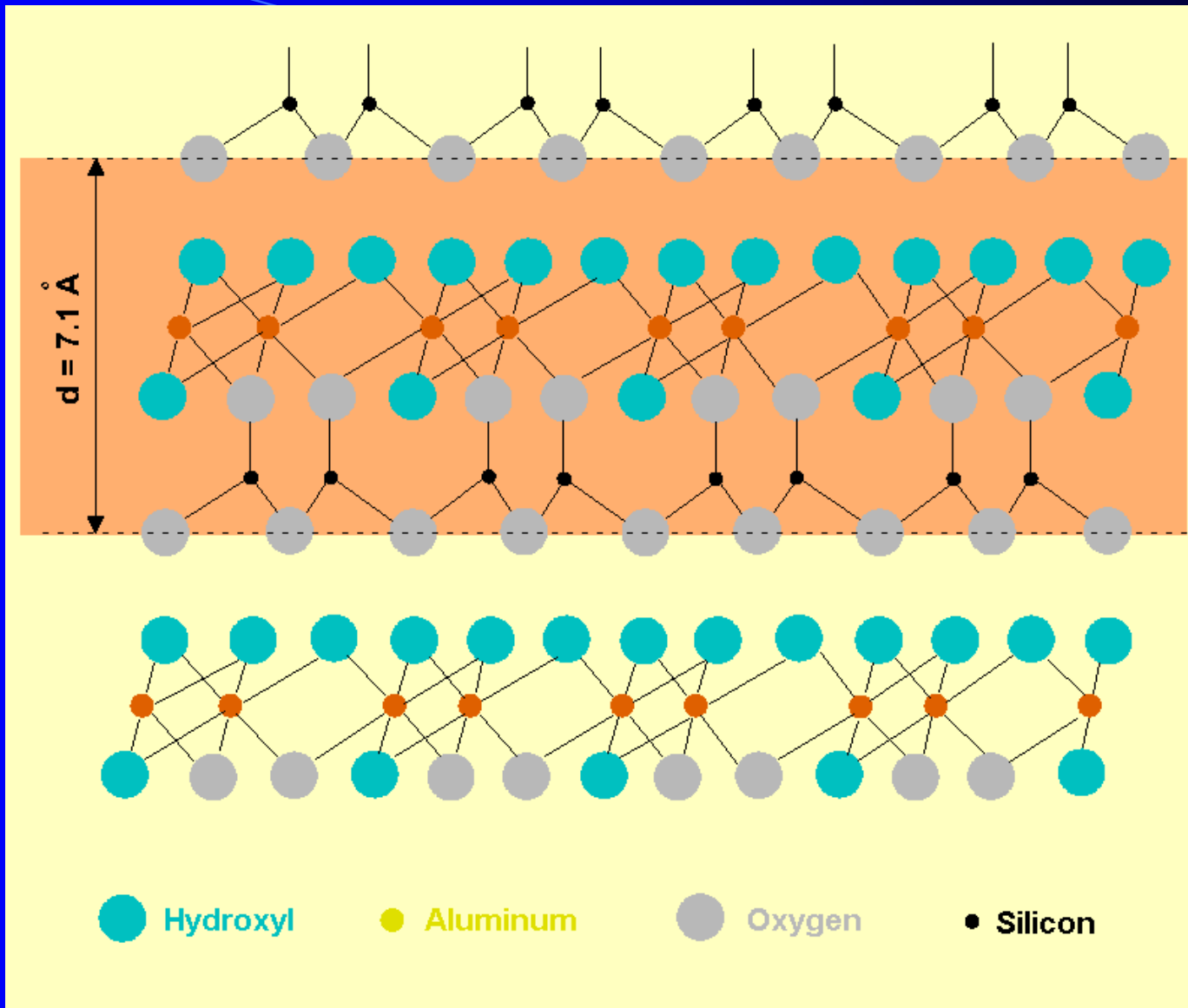


Figure 7-6. Structure of kaolinite. Each structural unit consists of a gibbsite layer and a tetrahedral layer. Note that only two out of three octahedral sites in the octahedral layer are occupied.

Table 7-6. Substitutions for smectite group clay minerals

| Mineral | Tetrahedral cations | Octahedral cations | Exchangeable cations |
|-----------------|-------------------------------------|--|-----------------------------|
| Di-octahedral | | | |
| Montmorillonite | Si ₈ | Al _{3.3} Mg _{0.7} | (0.5 Ca, Na) _{0.7} |
| Beidellite | Si _{7.3} Al _{0.7} | Al ₄ | (0.5 Ca, Na) _{0.7} |
| Nontronite | Si _{7.3} Al _{0.7} | Fe ₄ ³⁺ | (0.5 Ca, Na) _{0.7} |
| Tri-octahedral | | | |
| Saponite | Si _{7.2} Al _{0.8} | Mg ₆ | (0.5 Ca, Na) _{0.8} |
| Hectorite | Si ₈ | Mg _{5.3} Li _{0.7} | (0.5 Ca, Na) _{0.7} |
| Sauconite | Si _{6.7} Al _{1.3} | Zn ₄₋₆ (Mg, Al, Fe ³⁺) ₂₋₀ | (0.5 Ca, Na) _{0.7} |

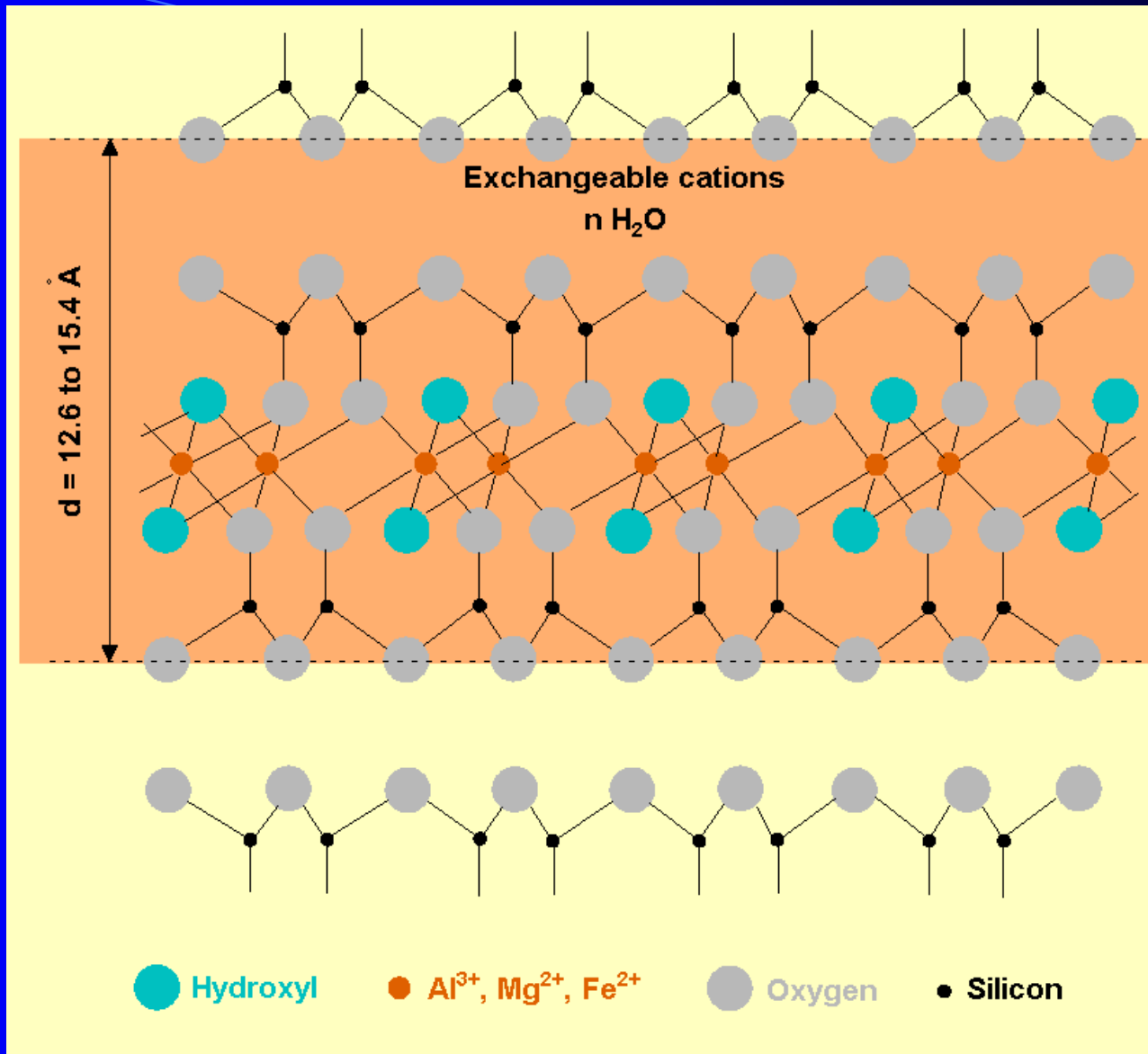


Figure 7-7. Structure of montmorillonite, a 2:1 clay. The octahedral layer is a gibbsite layer. Substitution of Mg^{2+} for Al^{3+} in the octahedral layer is charge balanced by the addition of Na^+ or Ca^{2+} cations (exchangeable cations) in the interlayer position.

Table 7-7. Permanent negative surface charge of 2:1 clay mineral

| Mineral group | Charge (mol sites kg ⁻¹) ² |
|---------------|---|
| Kaolinite | 0.02 - 0.2 |
| Illites | 0.1 - 0.9 |
| Smectites | 0.7 - 1.7 |
| Vermiculites | 1.6 - 2.5 |

Table 7-8. Surface area per unit mass of illite with a density of 2600 kg m⁻³

| Length of side (m) | Number of cubes | Surface area of cube (m ²) | Surface area (m ² g ⁻¹) |
|--------------------------------|----------------------|--|--|
| 1 | 1 | 6 | 2.3 x 10 ⁻⁶ |
| 1 x 10 ⁻² (cm) | 1 x 10 ⁶ | 6 x 10 ⁻⁴ | 2.3 x 10 ⁻⁴ |
| 1 x 10 ⁻⁶ (1 μm) | 1 x 10 ¹⁸ | 6 x 10 ⁻¹² | 2.31 |
| 1 x 10 ⁻⁷ (0.1 μm) | 1 x 10 ²¹ | 6 x 10 ⁻¹⁴ | 23.1 |
| 1 x 10 ⁻⁸ (0.01 μm) | 1 x 10 ²⁴ | 6 x 10 ⁻¹⁶ | 231 |

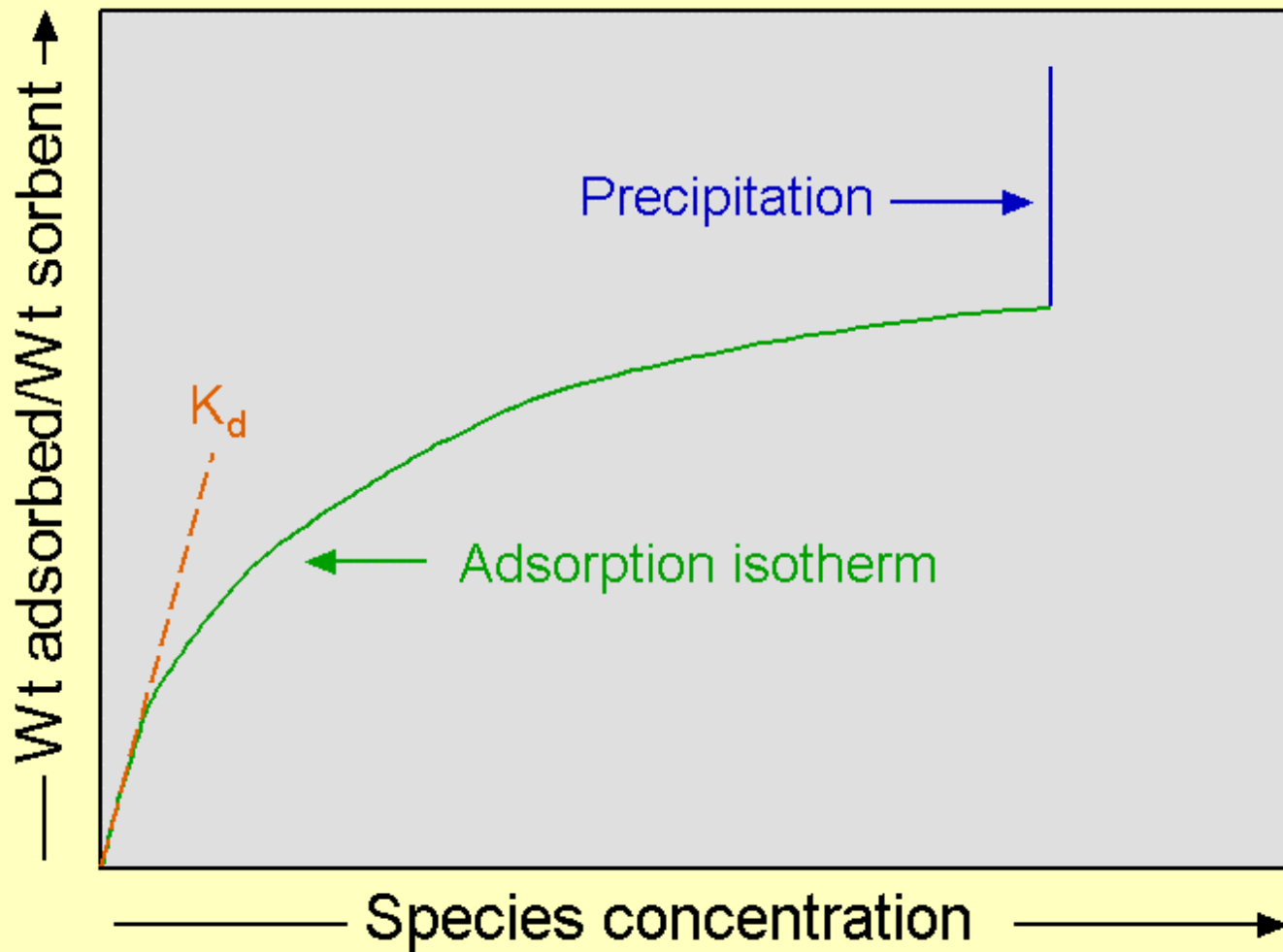


Figure 7-8. Representation of a typical adsorption isotherm showing the distribution of a species between an aqueous phase and a solid (sorbent). At very low concentrations, the distribution behaves ideally and can be represented by a unique value, K_d . At higher concentrations, the partitioning deviates from ideality. If precipitation occurs, the concentration of the species in solution will remain constant; i.e., the solution is saturated with respect to the particular species.

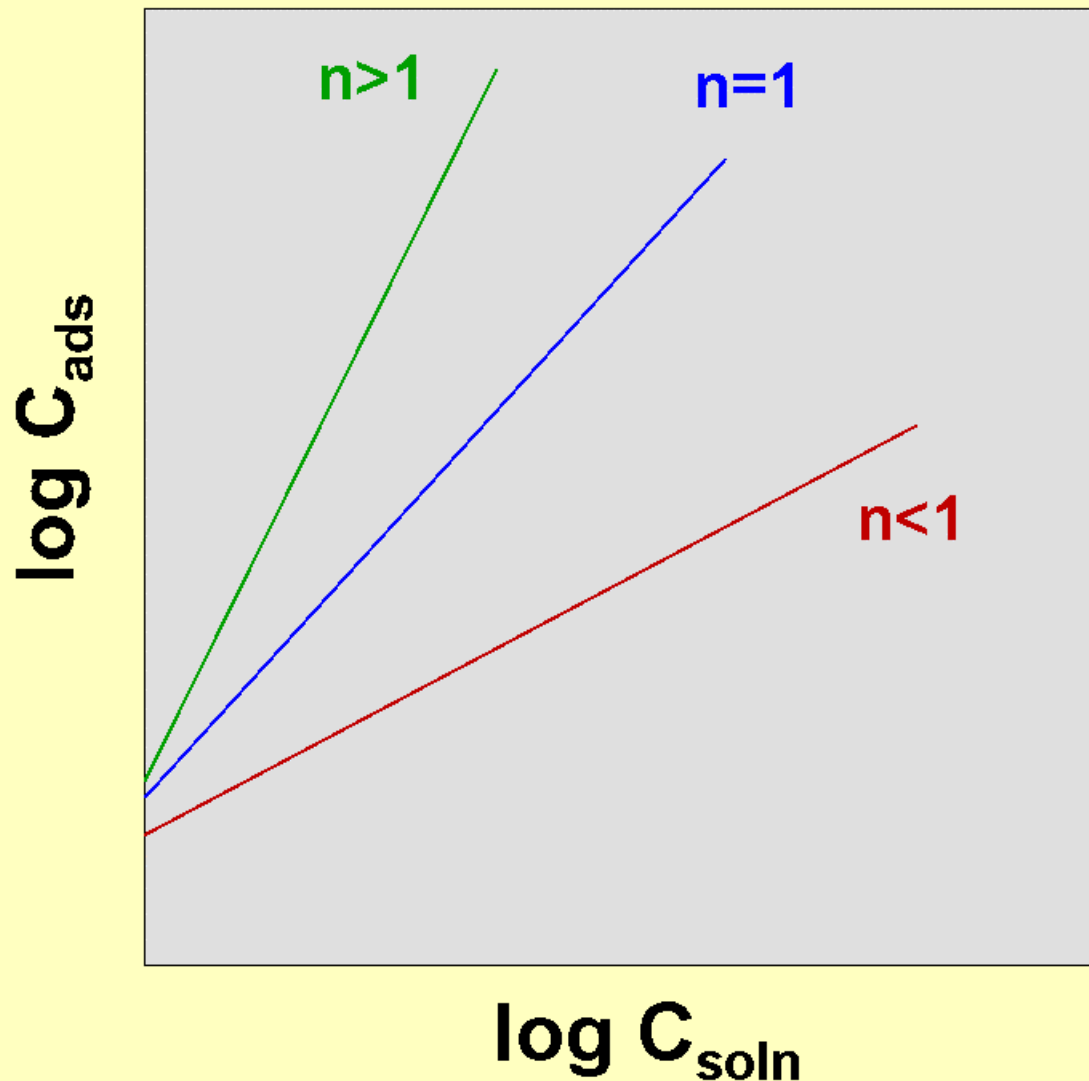


Figure 7-9. Plot of the log of the concentration of the substance adsorbed on a particle (C_{ads}) versus the log of the concentration of the substance in water (C_{soln}). Linear plots indicate that the partitioning can be represented by a Freundlich isotherm. The slope of the line gives the exponent, n , and the intercept gives the value for $\log K$.

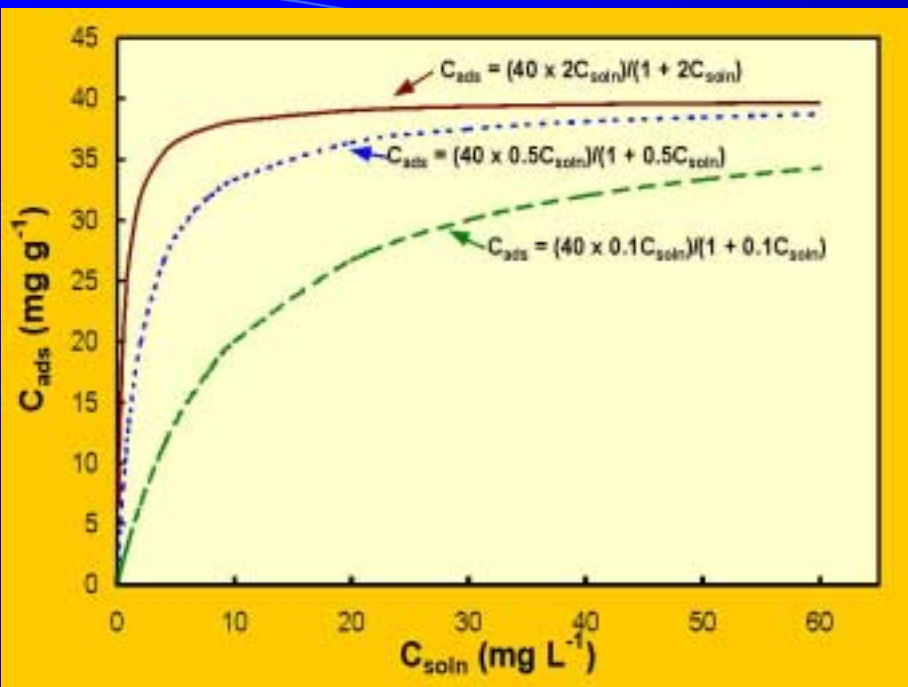


Figure 7-10a. Langmuir isotherms for $Q^o = 40 \text{ mg g}^{-1}$ and $K = 0.1, 0.5, \text{ and } 2$.

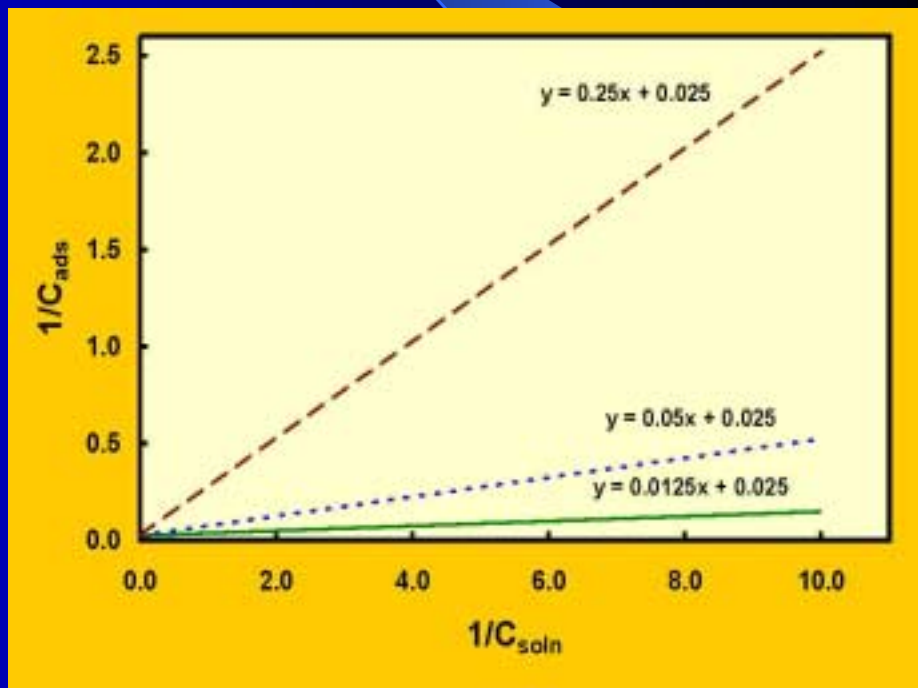


Figure 7-10b. Linearized form of the isotherms plotted in Figure 7-10a. The y-intercept is $1/Q^o$ and the slope = $1/KQ^o$.

Table 7-9. Chemical formulas and various properties of representative natural zeolites

| Mineral | Representative chemical formula | Si:(Si+Al) | Void space | Free aperture size |
|----------------|---|------------|------------|--|
| Erionite | $\text{NaK}_2\text{MgCa}_{1.5}(\text{Al}_8\text{Si}_{28})\text{O}_{72}\cdot 28\text{H}_2\text{O}$ | 0.75-0.78 | 0.36 | 3.6Å x 5.2Å 8-rings \perp (001) |
| Mordenite | $\text{Na}_3\text{KCa}_2(\text{Al}_8\text{Si}_{40})\text{O}_{96}\cdot 8\text{H}_2\text{O}$ | 0.80-0.85 | 0.26 | 6.7Å x 7.0 Å 12-rings \parallel (001) 2.9Å x 5.7Å 8-rings \parallel (010) |
| Clinoptilolite | $(\text{Na},\text{K})_6(\text{Al}_6\text{Si}_{30})\text{O}_{72}\cdot 20\text{H}_2\text{O}$ | 0.74-0.84 | 0.34 | 3.5Å x 7.9Å 10-rings \parallel (001) 3.0Å x 4.4Å 8-rings |
| Phillipsite | $\text{K}_2(\text{Ca}_{0.5},\text{Na})_4(\text{Al}_6\text{Si}_{10})\text{O}_{32}\cdot 12\text{H}_2\text{O}$ | 0.54-0.75 | 0.30 | 4.2Å x 4.4Å 8-rings \parallel (100) 2.8Å x 4.8Å 8-rings \parallel (010) 3.3Å diameter 8-rings \parallel (001) |
| Chabazite | $\text{Ca}_2(\text{Al}_4\text{Si}_8)\text{O}_{24}\cdot 12\text{H}_2\text{O}$ | 0.59-0.80 | 0.48 | 3.7Å x 4.1Å 8-rings |

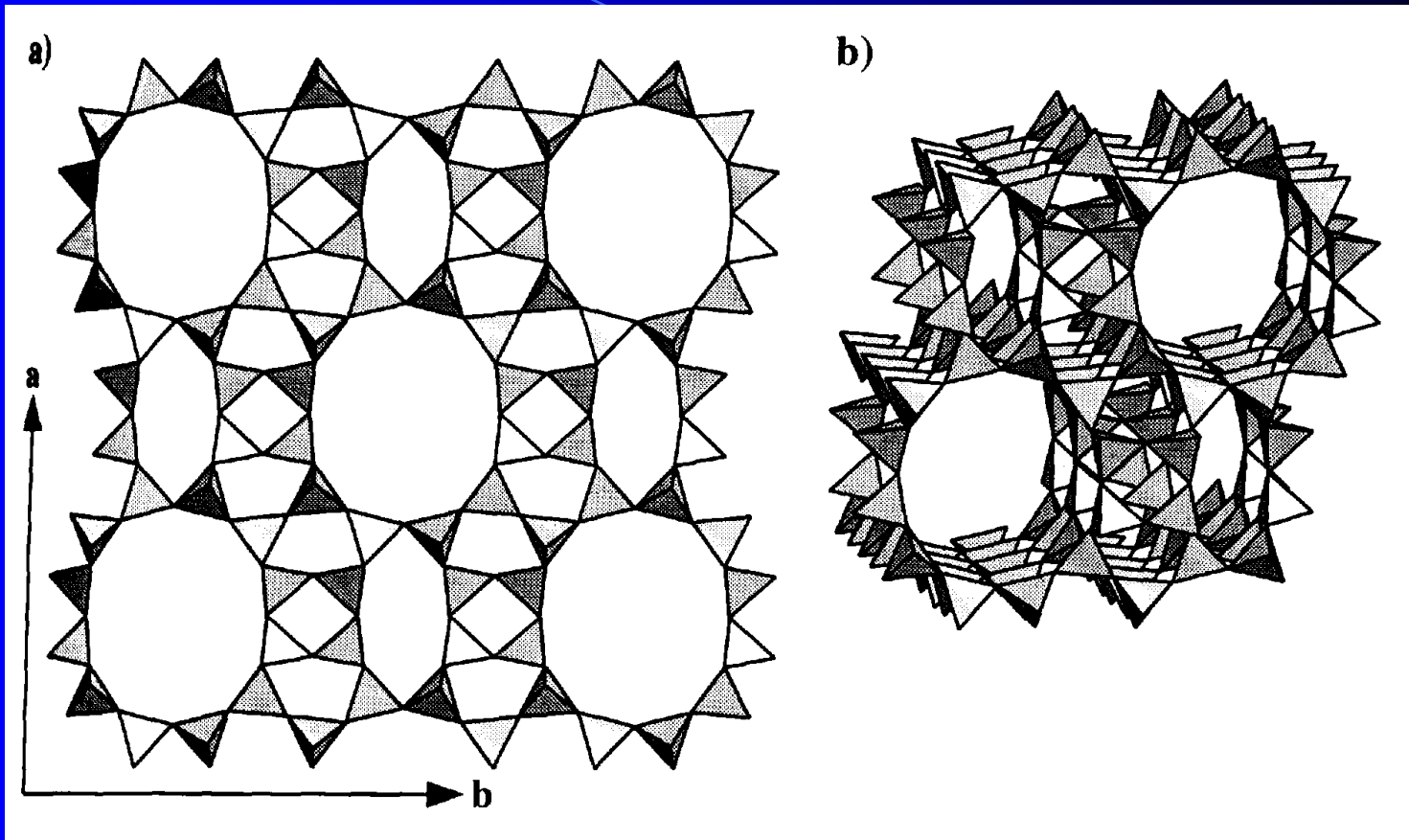


Figure 7-11. The structure of mordenite viewed (a) down the c -axis and (b) obliquely down the c -axis. Note the presence of two sets of channels, one consisting of 12-membered rings and the other of 8-membered rings (count the tetrahedra around the large and small channels). From Bish and Guthrie (1993).

Table 7-10. Theoretical cation-exchange capacity for selected zeolite minerals

| Zeolite | Typical Unit-Cell Formula | CEC (meq/100 g) |
|----------------|---|--------------------|
| Analcime | $\text{Na}_{16}(\text{Al}_{16}\text{Si}_{32}\text{O}_{96}) \cdot 16\text{H}_2\text{O}$ | 450 |
| Chabazite | $\text{Ca}_2(\text{Al}_4\text{Si}_8\text{O}_{24}) \cdot 12\text{H}_2\text{O}$ | 390 |
| Clinoptilolite | $(\text{Na},\text{K})_6(\text{Al}_6\text{Si}_{30}\text{O}_{72}) \cdot 20\text{H}_2\text{O}$ | 220 |
| Erionite | $\text{NaK}_2\text{MgCa}_{1.5}(\text{Al}_8\text{Si}_{28}\text{O}_{72}) \cdot 28\text{H}_2\text{O}$ | 280 |
| Faujasite | $\text{Na}_{20}\text{Ca}_{12}\text{Mg}_8(\text{Al}_{60}\text{Si}_{32}\text{O}_{384}) \cdot 235\text{H}_2\text{O}$ | 360 |
| Ferrierite | $(\text{Na},\text{K})\text{Mg}_2\text{Ca}_{0.5}(\text{Al}_6\text{Si}_{30}\text{O}_{72}) \cdot 20\text{H}_2\text{O}$ | 230 |
| Heulandite | $(\text{Na},\text{K})\text{Ca}_4(\text{Al}_9\text{Si}_{27}\text{O}_{72}) \cdot 24\text{H}_2\text{O}$ | 320 |
| Lau montite | $\text{Ca}_4(\text{Al}_8\text{Si}_{16}\text{O}_{48}) \cdot 16\text{H}_2\text{O}$ | 430 |
| Mordenite | $\text{Na}_3\text{KCa}_2(\text{Al}_8\text{Si}_{40}\text{O}_{96}) \cdot 28\text{H}_2\text{O}$ | 220 |
| Natrolite | $\text{Na}_{16}(\text{Al}_{16}\text{Si}_{24}\text{O}_{80}) \cdot 16\text{H}_2\text{O}$ | 530 |
| Phillipsite | $\text{K}_2(\text{Ca}_{0.5},\text{Na})_4(\text{Al}_6\text{Si}_{10}\text{O}_{32}) \cdot 12\text{H}_2\text{O}$ | 450 |
| Wairakite | $\text{Ca}_8(\text{Al}_{16}\text{Si}_{32}\text{O}_{96}) \cdot 16\text{H}_2\text{O}$ | 460 |

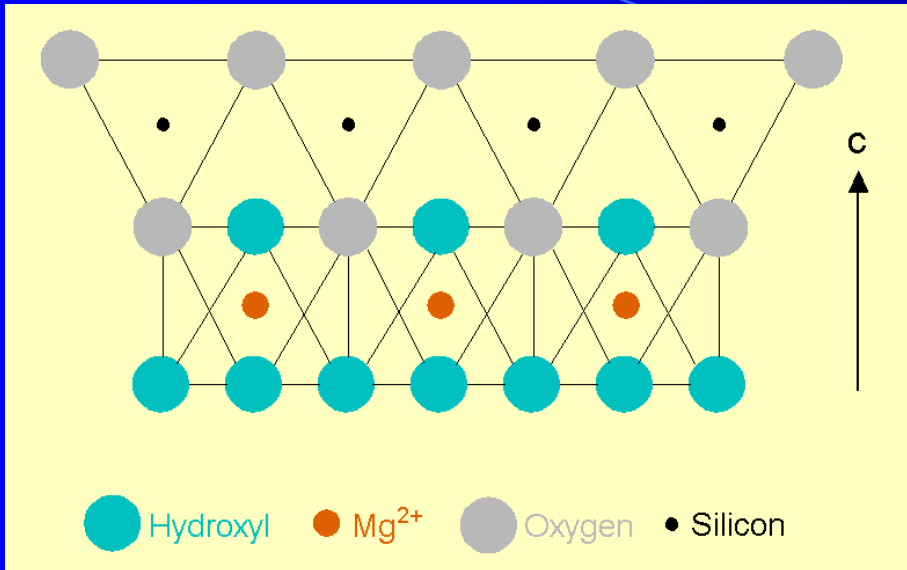


Figure 7-12. Crystal structure of chrysotile, a 1:1 layer silicate consisting of a tetrahedral layer and an octahedral layer in which Mg²⁺ ions are surrounded by four OH molecules and two oxygens.

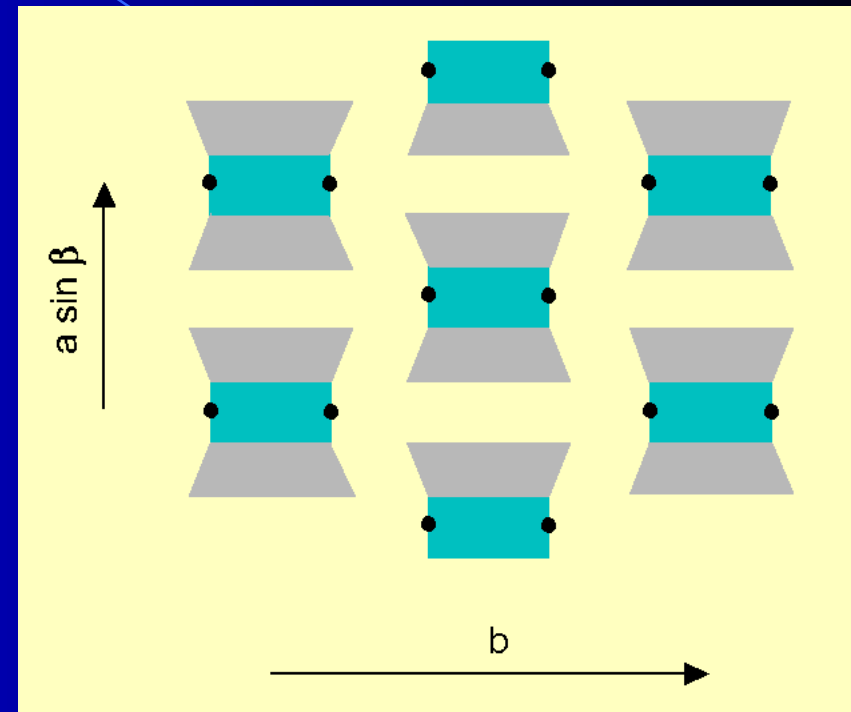


Figure 7-13. Simplified clinoamphibole structure looking down the *c*-axis. The gray areas are the tetrahedral chains, the cyanide area is the octahedral layer, and the filled circles indicate the M4 cation positions.

Table 7-11. Chemical formulas and properties of asbestos minerals

| Mineral | Chemical formula | Crystal system | Hardness | Specific gravity |
|---------------|--|----------------|-----------|------------------|
| Chrysotile | $Mg_3[Si_2O_5](OH)_4$ | Monoclinic | 2.5 | ≤ 2.55 |
| Actinolite | $Ca_2(Mg, Fe^{2+})_5[Si_8O_{22}](OH)_2$ | Monoclinic | 5 - 6 | 3.0 - 3.2 |
| Amosite | $(Fe^{2+}, Mg)_7[Si_8O_{22}](OH)_2$ | Monoclinic | 5.5 - 6.0 | 3.1 - 3.25 |
| Anthophyllite | $(Mg, Fe^{2+})_7[Si_8O_{22}](OH)_2$ | Orthorhombic | 5.5 - 6.0 | 2.85 - 3.1 |
| Crocidolite | $Na_2Fe^{3+}_2(Fe^{2+}, Mg)_3[Si_8O_{22}](OH)_2$ | Monoclinic | 5 | 3.15 - 3.5 |
| Tremolite | $Ca_2Mg_5[Si_8O_{22}](OH)_2$ | Monoclinic | 5 - 6 | 2.9 - 3.2 |

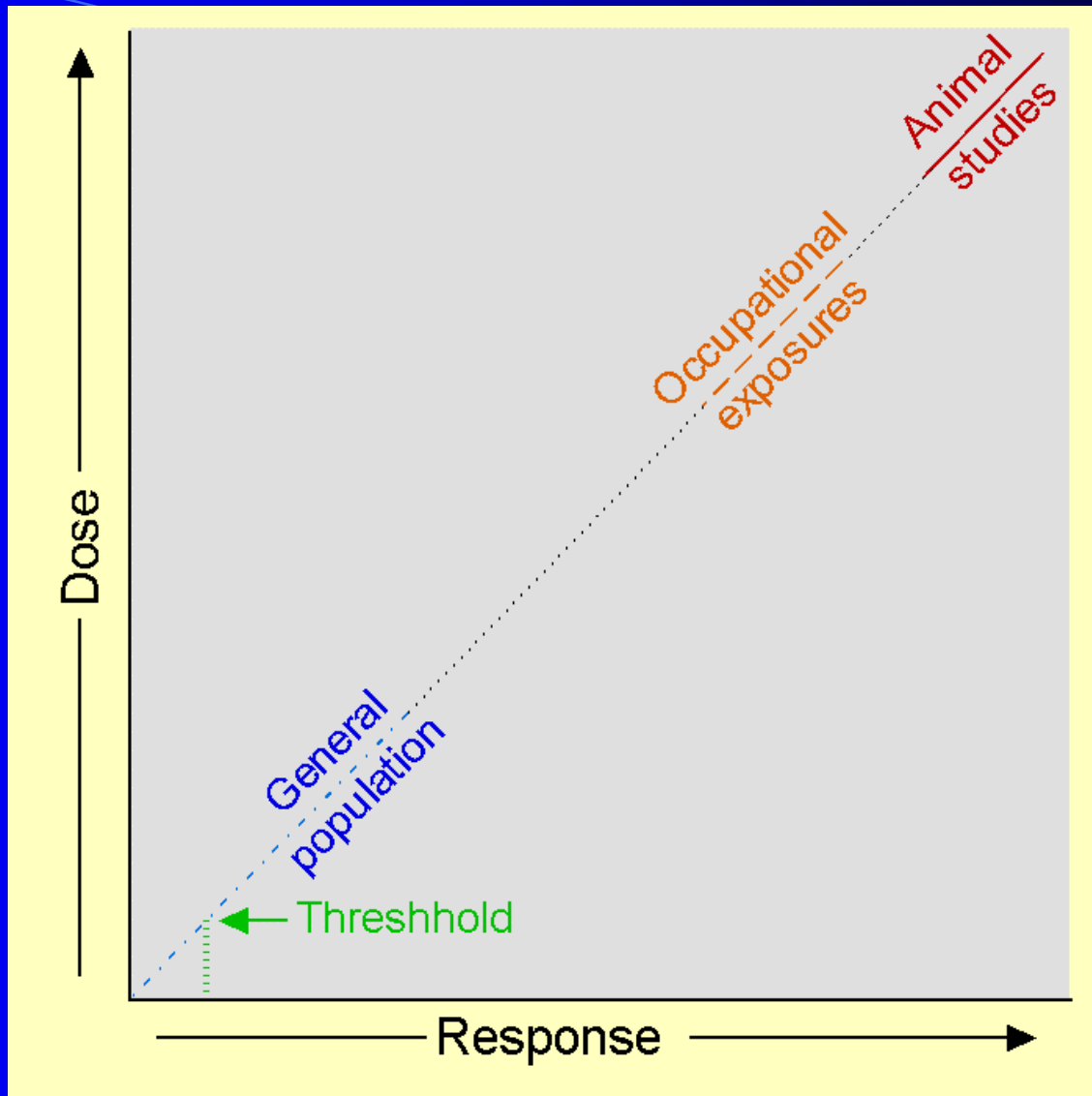


Figure 7-14. Schematic representation of the relationship between dose and response for a particular contaminant. Linear extrapolation to zero is often done based on animal studies and occupational exposures. The threshold dose implies that there is some dose below which no change in response is observed.

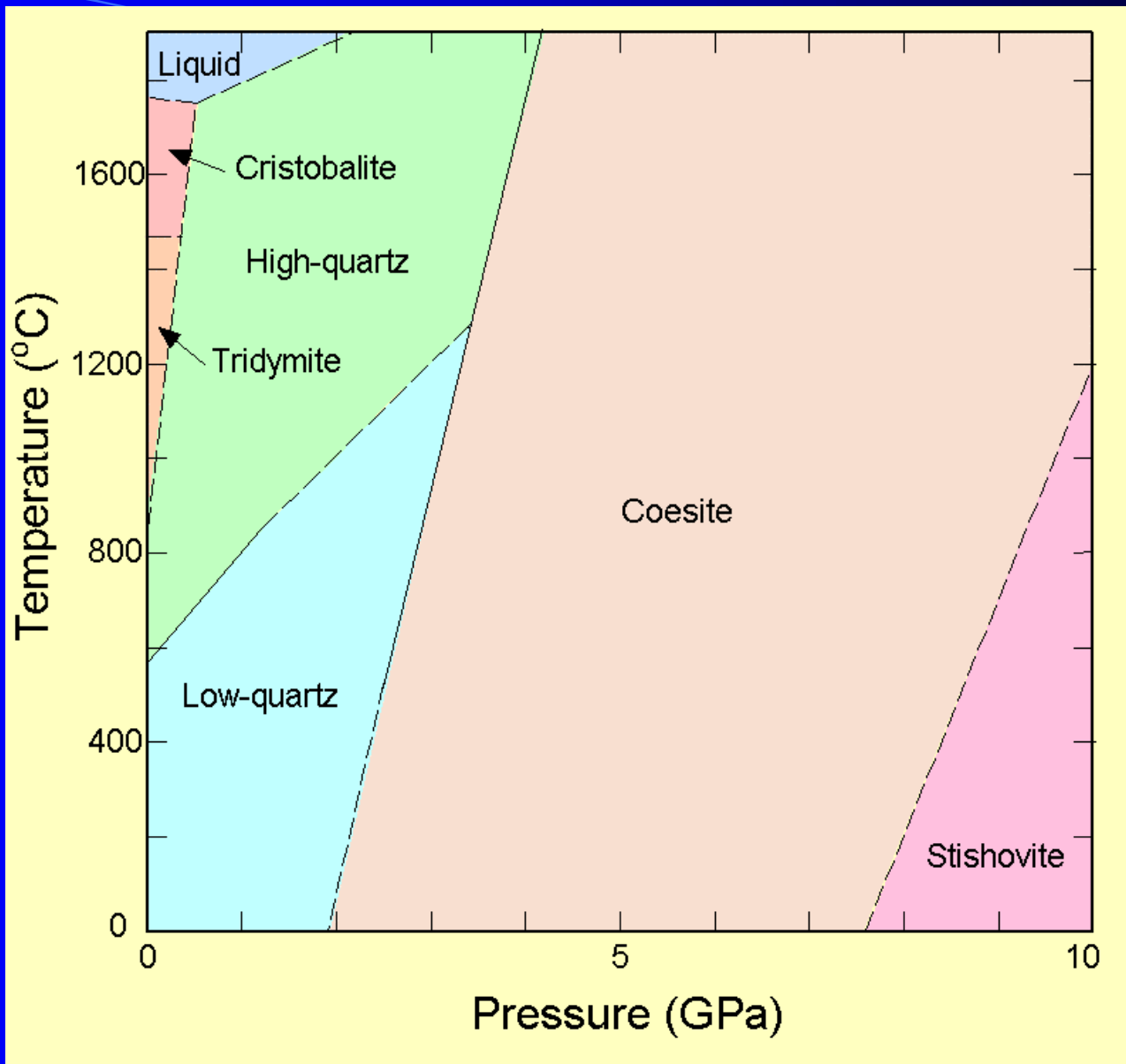


Figure 7-15. Phase diagram for the silica system Adapted from MANUAL OF MINERALOGY, 21/e by C. Klein and C. S. Hurlbut, p. 681. Copyright © 1993. This material is used by permission of John Wiley & Sons, Inc.

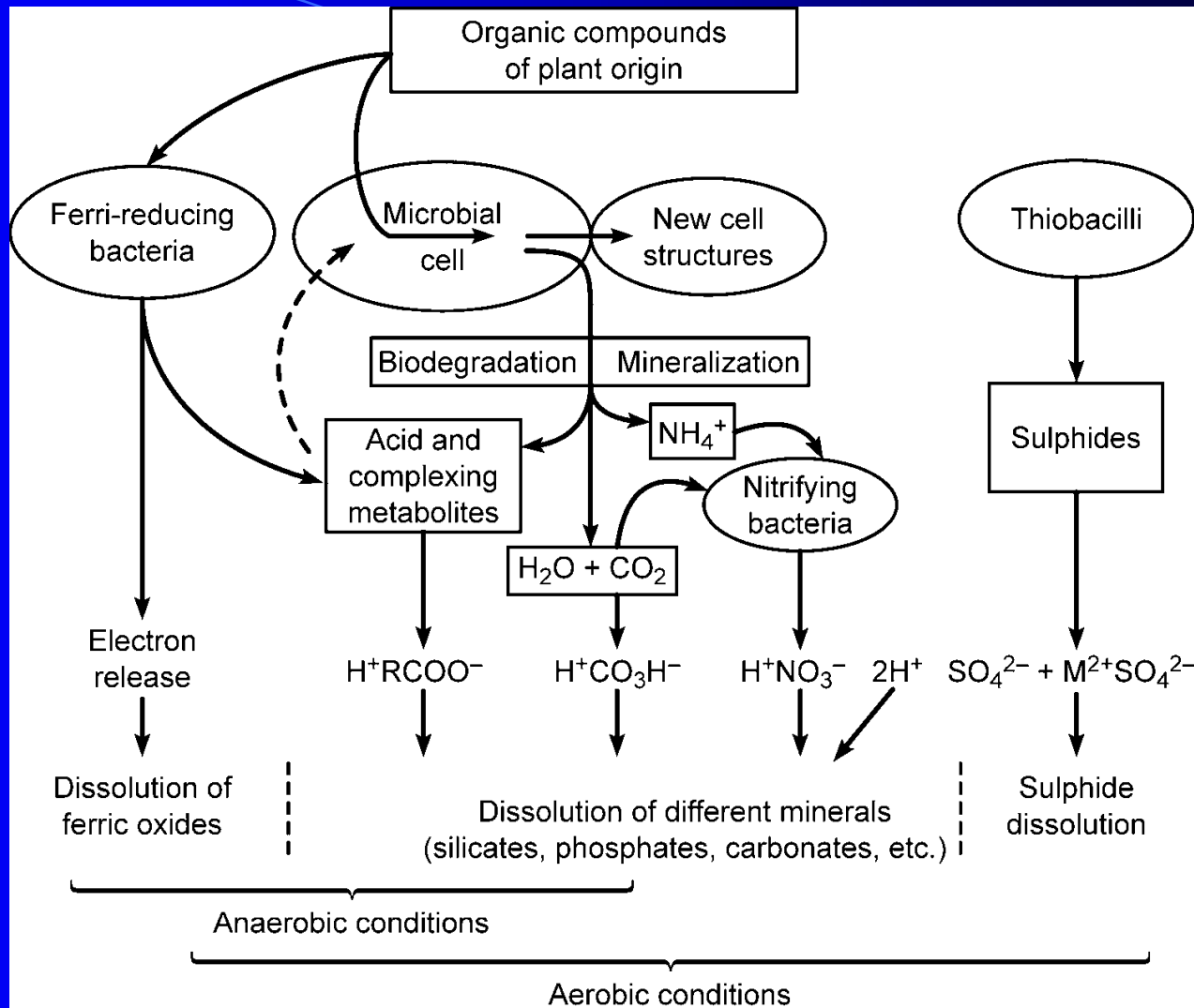


Figure 7-16. Various pathways for the dissolution and weathering of minerals by soil microorganisms. Note both the energy sources and products of the various pathways. See text for further discussion. From Berthelin et al. (2000).

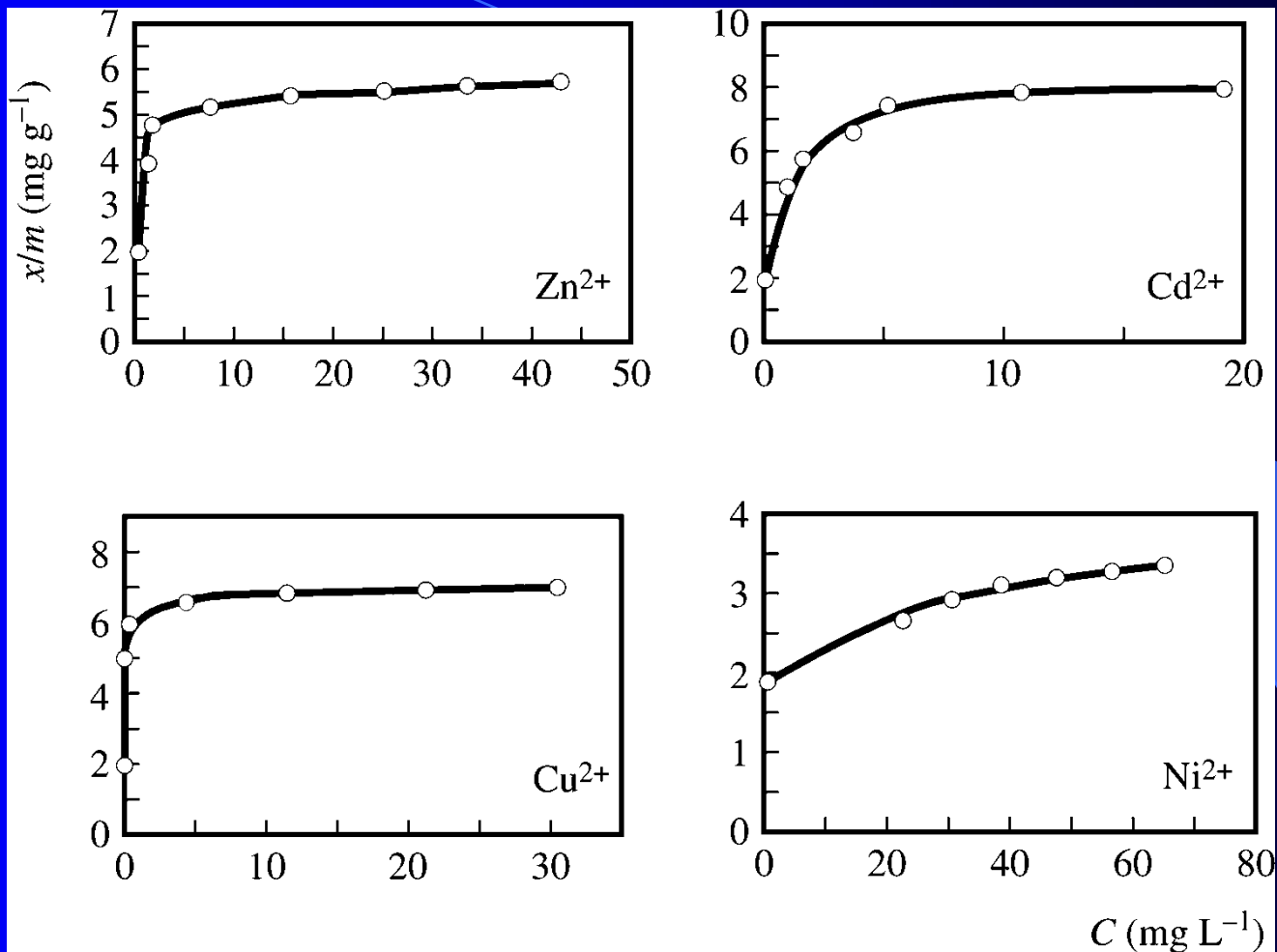


Figure 7-C2-1. Adsorption isotherms for sepiolite. Adsorbent dose = 10 g L⁻¹, agitation time = 3 h, pH = 4, and T = 22°C. The Langmuir equation provided the best fit to the adsorption isotherms. From Sanchez et al. (1999).

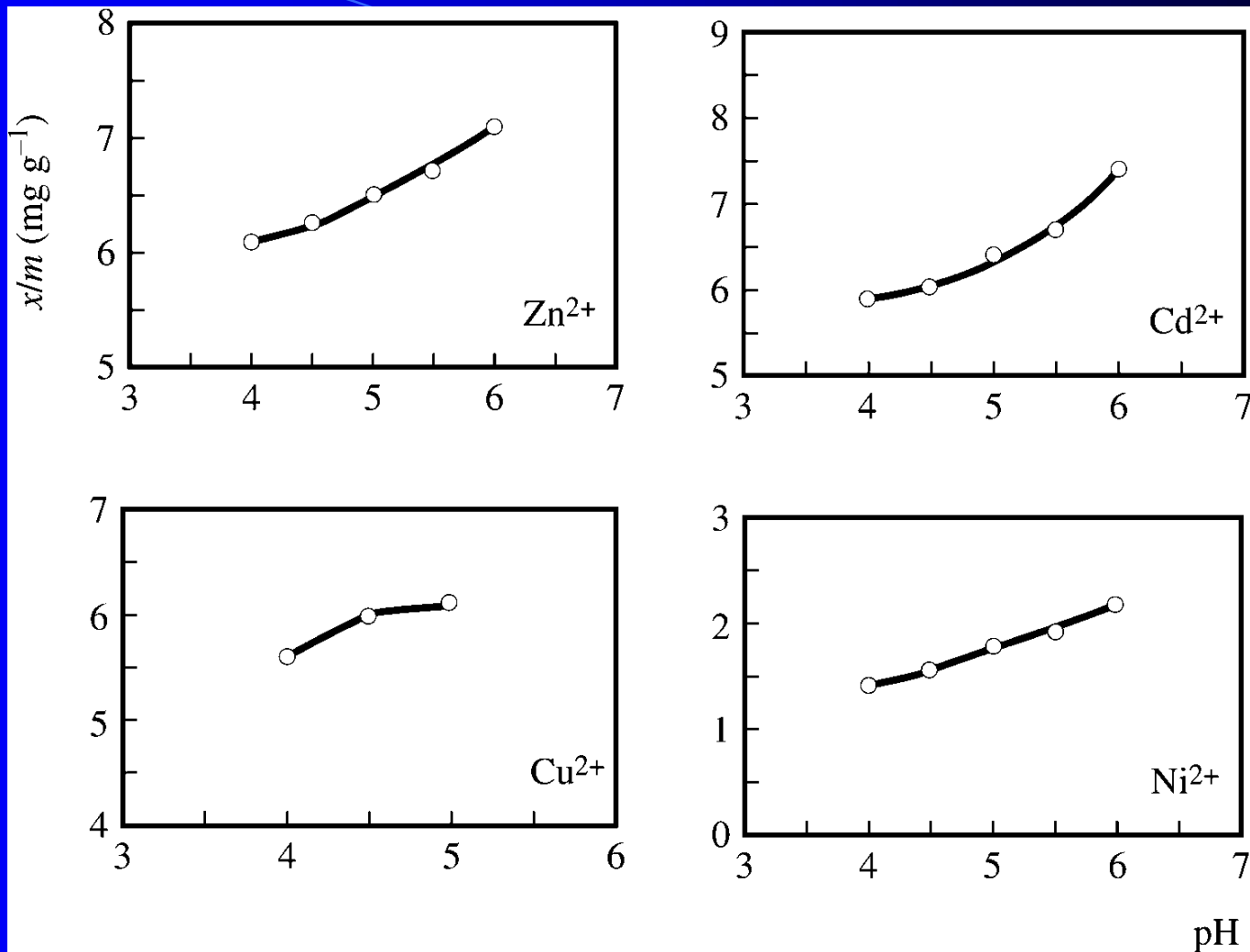


Figure 7-C2-2. Effect of pH on the adsorption of metal cations by sepiolite. Adsorbent dose = 5 g L^{-1} , initial cation concentration = 50 mg L^{-1} , agitation time = 2 h. With increasing pH the adsorption of the metal ions increases. From Sanchez et al. (1999).

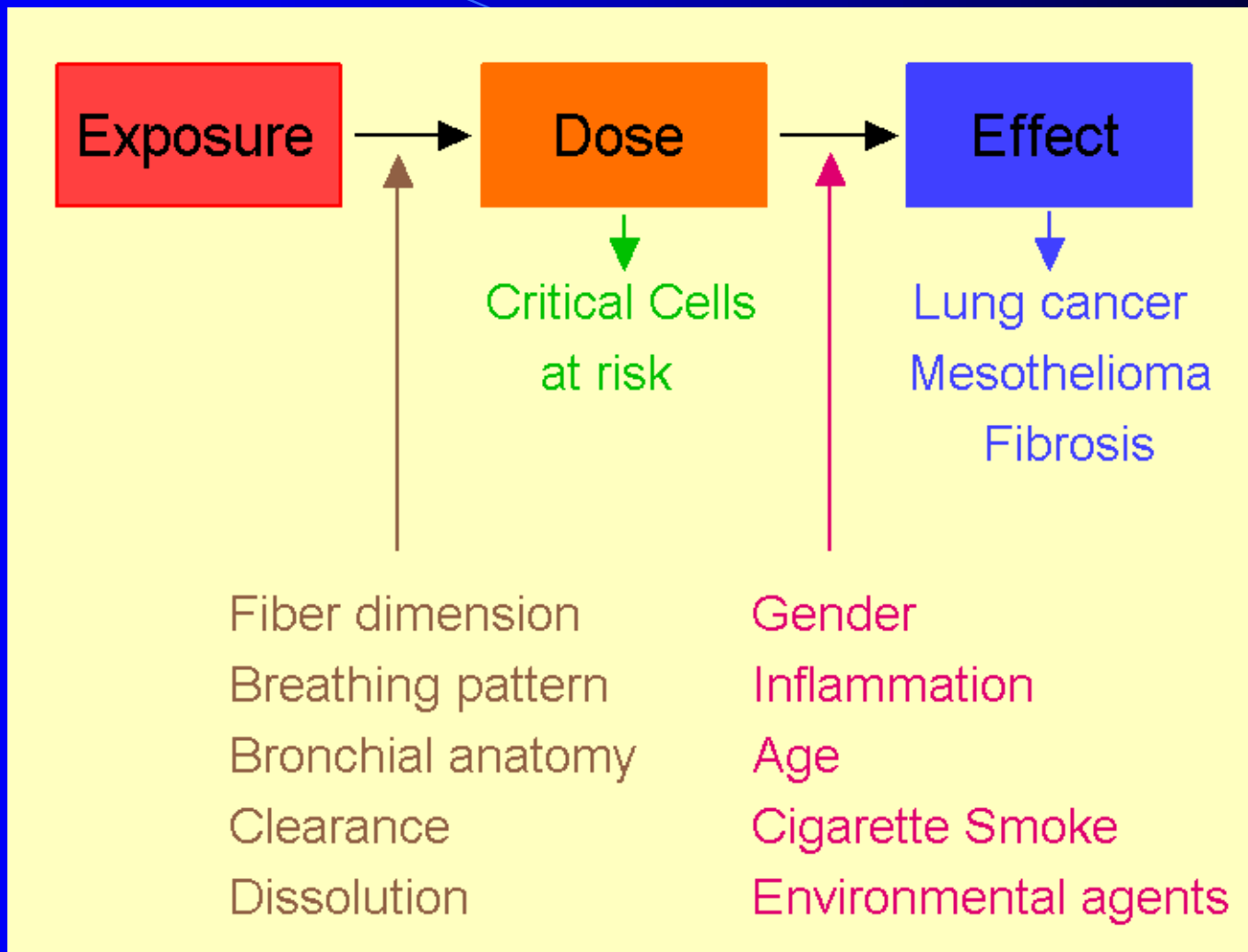


Figure 7-C4-1. Schematic diagram showing the various factors that affect the relationship among exposure-dose-effect. Adapted from Johnson and Mossman (2001).

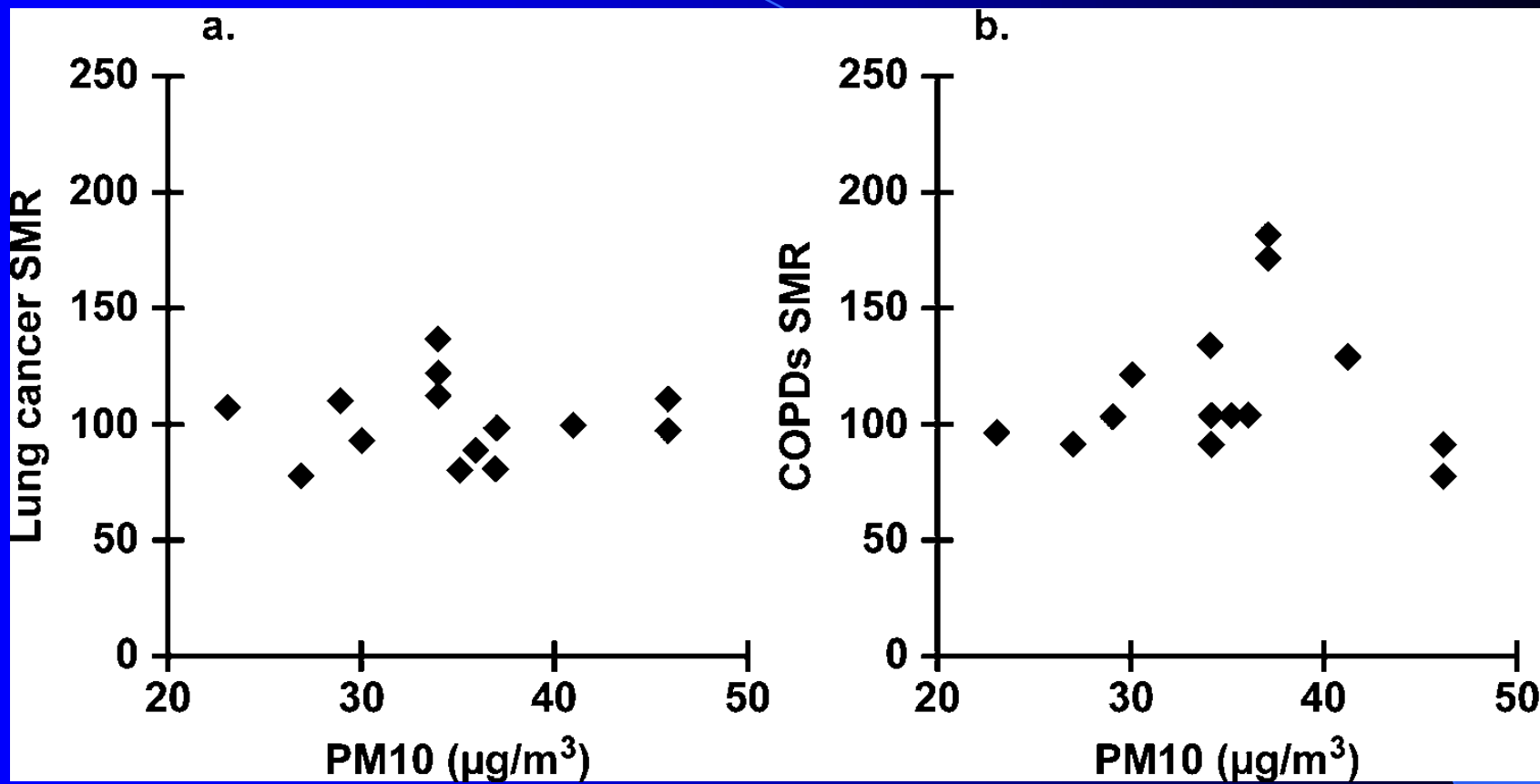


Figure 7-C5-1. Plots of PM10 versus (a) adjusted (age and smoking) lung cancer SMR and (b) adjusted (age) COPDs. From Norton and Gunter (1999).